Synthesis and Structural Characterization of Dendritic-Linear PMA-APM-r-PS Copolymers for a Self-Assembled Microporous Matrix

SHANG-JU HSIEH,[1] CHENG-CHIEN WANG,[2] CHUH-YUNG CHEN[1]

[1]Department of Chemical Engineering, National Cheng Kung University, Tainan 70101, Taiwan

[2]Department of Chemical and Materials Engineering, Southern Taiwan University, Tainan 710, Taiwan

Received 21 January 2010; accepted 29 April 2010
DOI: 10.1002/pola.24113
Published online in Wiley InterScience (www.interscience.wiley.com).

ABSTRACT: A set of dendritic-linear copolymers, poly(maleic anhydride-grafted-3,3′-dimethyl-(4-aminophenylazanediyl)bis(2-methylpropanoate))-random-polystyrene (PMA-APM-r-PS), was successfully prepared by copolymerization of the novel dendritic macromonomer, 4-(4-(bis(3-(4-(bis(3-methoxy-2-methyl-3-oxopropyl)amino)phenylamino)-2-methyl-3-oxopropyl)amino)phenylamino)-4-oxobut-2-enoic acid (MA-APM), with styrene monomer. The dendritic MA-APM macromonomer dendron 3,3′-dimethyl-(4-aminophenylazanediyl)bis(2-methylpropanoate) (APM) was then grafted by using the divergent growth method. FTIR, ^{1}H NMR, and ^{13}C NMR spectra were used to identify the structures of the dendron, the dendritic macromonomer, and the dendritic-linear PMA-APM-r-PS copolymer. Furthermore, microporous dendritic-linear PMA-APM-r-PS copolymer films were prepared by using solvent-induced phase separation at room temperature. We investigated the phase separation behavior and morphological structures of the dendritic-linear copolymer film as functions of dendritic GMA-HPAM segments in the content using SEM. Self-assembly of the dendritic-linear PMA-APM-r-PS copolymer in the MG2-X system, which represented the second generation dendron containing X wt % of the dendritic MA-APM segment, resulted in submicron phase segregation. Interestingly, the submicron phase segregation morphology of the MG2–43 sample presented a uniform size distribution of ordered-array structures. The results of this study demonstrate that controlling the appropriate macromonomer content via the grafting of a three-dimensional structure results in a self-assembly process that is capable of providing an ordered-array microporous morphology in a polymer film. © 2010 Wiley Periodicals, Inc. J Polym Sci Part A: Polym Chem 48: 3290–3301, 2010

KEYWORDS: dendrimers; dendritic-linear copolymer; hexagonally-ordered structure; macromonomers; self-assembly

INTRODUCTION Microporous thin film materials with perfect arrangements of ordered structures (10 μm $\geqq$ pore size $\geqq$ 50 nm) have attracted significant interest in recent year due to their great potential as templating materials,[1] membrane filters,[2] optical filters,[3] electronic and optical devices,[4–6] catalytic supports,[7] and biosensors.[8] Until recently the modes of preparation of these types of microporous materials were through the "top-down" approaches using photolithographic techniques[9] or through "bottom-up" approaches using the self-assembly of materials as templates around which material assemblies take place. In addition, the templating method and "breath figure" approach are two of the most widely used techniques for the fabrication of ordered microporous films through the "bottom-up" approach. In the templating method, uniform spherical particles (usually silica[10] or polymer spheres[11]) are used as a template, and ordered microporous structure films are formed when the templates are removed.[12,13] Alternatively, a template-free method called the "breath figure" approach, or water-assisted method, utilizes a moist air-flow to create microdroplets of water that work as a template for the micropores in condensing and self-assembling block copolymer solutions. After complete evaporation of the solvent, the water droplets remain in the copolymer films, forming a perfectly ordered microporous copolymer structure.[14–19] Many studies have discussed the structure of three-dimensional films and submicron films by means of the water-assisted method, and according to their results, the pore sizes of the ordered structures are influenced by several key factors, such as the properties of the block copolymer and the relative humidity and air-flow velocity. Film preparation is challenging because of the need for a special block copolymer polymerization treatment.

Dendronized, or dendritic-grafted copolymers, are linear polymers that bear pendant dendrons along the repeated units. The two main synthetic routes to dendronized copolymers include the "coupling to" approach and the "macromonomer" approach.[20,21] In the "coupling to" approach, the copolymer that becomes the core in the final product serves as a starting material. The anchor groups of the copolymer are used to either divergently or convergently attach a dense sequence of dendrons. In contrast, in the "macromonomer" approach, a monomer already carrying dendrons is subjected

Correspondence to: C.-Y. Chen (E-mail: ccy7@ccmail.ncku.edu.tw)
Journal of Polymer Science: Part A: Polymer Chemistry, Vol. 48, 3290–3301 (2010)

to polymerization or polycondensation. The obvious advantage of the "macromonomer" approach over the "coupling to" strategy lies in the fact that it does not involve a postpolymerization reaction, and can offer accurate control over the dendritic side groups,[22] however, it becomes difficult to get copolymers with higher degrees of polymerization (DP) for the dendritic macromonomers of three or greater generations due to steric hindrance. Nevertheless, one may say that, judging by the number of articles, polymerization using the "macromonomer" route is the most successful approach thus far. In addition, because of the steric hindrance imposed by the bulky dendritic side groups due to the rod-like shape of the copolymers, many microporous films are made using dendritic-linear copolymers. Xi et al.[23] have prepared honeycomb macroporous films on the basis of amphiphilic dendronized block copolymers using and on-solid surface spreading method and an on-water spreading method on the basis of the self-organization of water droplets. In addition, Ishizu et al.[24] have reported the fabrication of highly ordered microporous films using emulsion micelles of the amphiphilic PEO-*b*-PMMA diblock copolymer using the current water-assisted method.[24]

More recently, we have demonstrated a new method for constructing hexagonally-ordered microporous matrices using dendritic-linear random copolymers via solvent-induced phase separation.[25] According to our results, the micelle domains and the interaction of each segment in the dendritic-linear copolymer control the surface morphology of the matrix. Therefore, controlling the appropriate macromonomer content by grafting three-dimensional structures can directly promote self-assembly and provide a hexagonally ordered microporous matrix.

In this study, we announce the synthesis and characterization of the dendritic macromonomer, 4-(4-(bis(3-(4-(bis(3-methoxy-2-methyl-3-oxopropyl)amino)phenylamino)-2-methyl-3-oxopropyl)amino)phenylamino)-4-oxobut-2-enoic acid (MA-APM), and the dendritic-linear copolymer, 3,3′-dimethyl-(4-aminophenylazanediyl)bis(2-methylpropanoate))-random-polystyrene (PMA-APM-r-PS) (PMA-APM-r-PS). In addition, various microporous films over an area of more than 2 cm^2 were created via solvent-induced phase separation[26,27] and the morphologies of these copolymer films were characterized using scanning electron microscopy (SEM). Furthermore, we demonstrate how a hexagonally-ordered microporous structure with a 1.9–2.5 μm micropore size can form on the film surface of a dendritic-linear copolymer. We investigated the influence of the dendritic segment to the dendritic-linear copolymer system weight ratio on the number of ordered/disordered states, the number density of micropores, and the uniformity of the micropore size. We demonstrate that this experimental process is significantly different from the mechanism of microporous formation under moist air-flow conditions.

EXPERIMENTAL

Materials

Reagents were purchased from Aldrich and Fluka Co. and used without further purification. Maleic anhydride (MA) and *p*-phenylenediamine (*p*-PDA) were used as received. Styrene and methyl methacrylate (MMA) (Merck Co.) were purified using a distillation method under reduced pressure. They were stored at 5 °C before use.

Polymerization Procedure for the Dendritic-Linear Copolymer

Synthesis of the 4-(4-(bis(3-(4-(bis(3-methoxy-2-methyl-3-oxopropyl)amino)phenylamino)-2-methyl-3-oxopropyl)amino)phenylamino)-4-oxobut-2-enoic Acid (MA-APM) Macromonomer

The macromonomer 4-(4-(bis(3-(4-(bis(3-methoxy-2-methyl-3-oxopropyl)amino)phenylamino)-2-methyl-3-oxopropyl)amino)-phenylamino)-4-oxobut-2-enoic acid (MA-APM) was synthesized as part of this study. A solution of maleic anhydride (MA) in DMF was added dropwise to a vigorously stirred solution of *p*-phenylenediamine in DMF under a nitrogen atmosphere at 0 °C. Next, the mixture was stirred for 30 min at 0 °C and then further stirred for 24 h at room temperature. The feed ratio of *p*-phenylenediamine to MA was 10:1 (molar ratio). After reaction was complete, the solvent was removed under a reduced pressure at 60 °C using a rotary evaporator, and the resulting black powder was extracted by the mixed solution of toluene and chloroform, the ratio of toluene to chloroform was 1.5:1 (volumetric ratio), three times. After filtration, the solvent was removed under reduced pressure at room temperature by using rotary evaporator, and the resulting gray power was dried in a vacuum oven overnight to yield the final amine-terminated product (MA-APM-G0.5). Yield: 77%. ^{1}H NMR (400MHz, $CDCl_3$, 300K, TMS, δ_H, ppm): 6.42 and 6.85 (s, 2H, —C*H*=C*H*—), 6.64 and 7.38 (m, 4H, —N—Ar*H*—N—), 8.05 (—N*H*). FTIR (KBr pellet, cm^{-1}): 1546 (NH, amide II), 1640 (C=C), 1658 (C=O, amide I), 1696 (C=O), 3200 (NH_2) 3400 (NH), 3600 (OH).

A solution of freshly distilled MMA in ethanol was added dropwise to the solution of MA-G0.5 precursor in methanol under a nitrogen atmosphere over a period of 2 h, which was then stirred for 1 hr at 0 °C. Next, the mixture was further stirred for 5 days at room temperature. The feed ratio of MMA to MA-APM-G0.5 was 10:1 (molar ratio). After reaction was complete, the solvent and unreacted MMA were removed under a reduced pressure at 40 °C using a rotary evaporator, and the resulting dark-brown oil was dried in a vacuum oven overnight to yield the final ester-terminated product (MA-APM-G1). Yield: 80%. ^{1}H NMR (400 MHz, $CDCl_3$, 300 K, TMS, δ_H, ppm): 1.26 (t, 6H, —CH_3), 2.57 (s, 2H, N—CH_2—C*H*(—CH_3)—CO—O—), 3.71 (s, 6H, —C(=O)—O—CH_3) 3.51 and 3.83 (m, 4H, Ar-N(—CH_2—)—CH_2—CH—), 6.42 and 6.85 (s, 2H, —C*H*=C*H*—), 6.89 and 7.41 (m, 4H, —N—Ar*H*—N—). FTIR (KBr pellet, cm^{-1}): 1546 (NH, amide II), 1640 (C=C), 1658 (C=O, amide I), 1700 (C=O), 1740 (C=O), 3400 (NH), 3600 (OH).

A solution of *p*-PDA in ethanol was added dropwise to the solution of MA-G1 precursor in methanol under a nitrogen atmosphere over a period of 2 h, which was then stirred for 1 h at 0 °C. Next, the mixture was further stirred for 5 days at room temperature. The feed ratio of *p*-phenylenediamine to MA-APM-G1 was 10:1 (molar ratio). After reaction was complete, the solvent was removed under a reduced pressure at

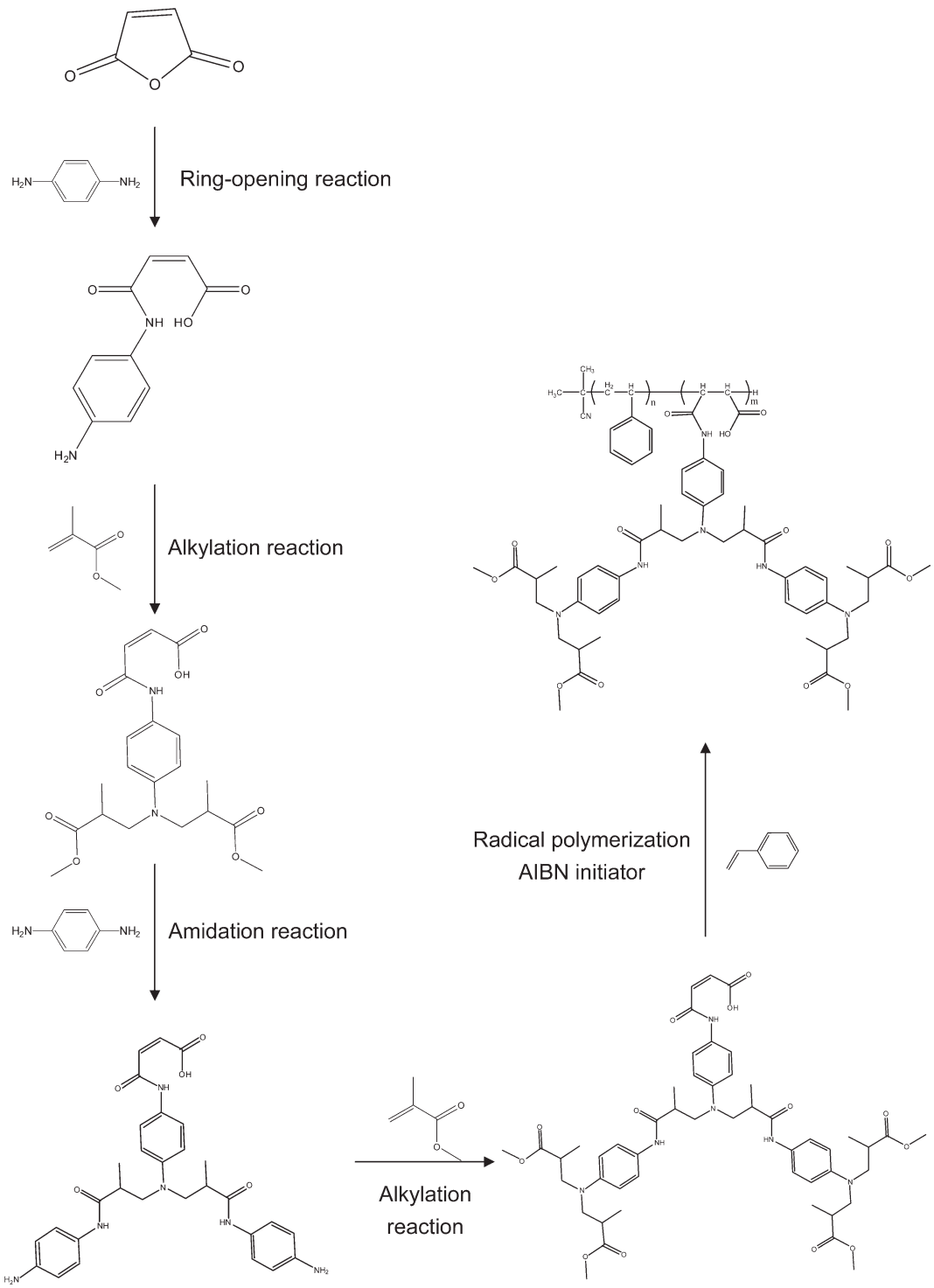

SCHEME 1

40 °C by using a rotary evaporator, and the resulting black power was extracted by the mixed solution of toluene and chloroform, the ratio of toluene to chloroform was 1:4 (volumetric ratio), three times. After filtration, the solvent was removed under reduced pressure at room temperature by using rotary evaporator, the resulting dark-brown oil was dried in a vacuum oven overnight to yield the final product (MA-APM-G1.5). Yield: 78%. ^{1}H NMR (400 MHz, $CDCl_3$, 300 K, TMS, δ_H, ppm): 1.28 (m, 18H, —CH_2—CH—CH_3), 2.57 (s, 2H, —CH_2—C*H*(—CH_3)—CO—), 3.52 and 3.81 (m, 4H, Ar-N—CH_2—CH—), 6.47 and 6.81 (s, 2H, —C*H*=C*H*—), 6.90 and 7.39 (m, 4H, —N—Ar*H*—N—). FTIR (KBr pellet, cm^{-1}): 1546 (NH, amide II), 1640 (C=C), 1658 (C=O, amide I), 1700 (C=O), 3200 (NH_2) 3400 (NH), 3600 (OH).

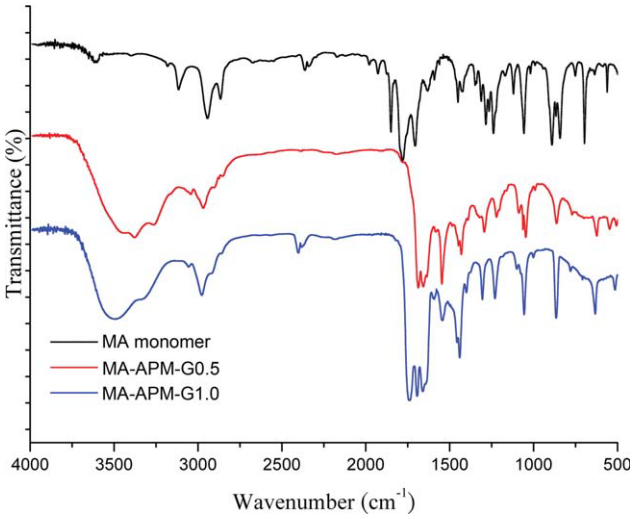

FIGURE 1 FTIR spectra of (a) MA monomer, (b) MA-APM-G0.5, and (c) MA-HPAM-G1.0. [Color figure can be viewed in the online issue, which is available at www.interscience.wiley.com.]

The intended product with higher generations of the MA-APM dendritic macromonomer was obtained by repeating the previous procedure.

Synthesis of the Dendritic-Linear Copolymer

The solution of the MA-APM macromonomer in *N*,*N*-dimethylacetamide was added dropwise to a three-neck 250 mL round-bottom flask, which contained the mixed solution of initiator, azobisisobutyronitrile (AIBN) and styrene monomer in *N*,*N*-dimethylacetamide, whereas mixing well in a nitrogen purge system. The mixture was stirred for 1 h at room temperature and then heated to 80 °C for 48 h. Finally, the dendritic-linear copolymers (PMA-APM-r-PS) were precipitated in a methanol solution, separated by filtration, and then dried in a vacuum oven. Yield: 85%. ^{1}H NMR (400 MHz, $CDCl_3$, 300 K, TMS, δ_H, ppm): 0.50–3.90 (m, —C*H*—, —CH_2—, —CH_3), 3.69 (m, —CO—O—CH_3), 6.65–7.45 (m, benzene), 7.08 (m, —CO—N*H*—).

The overall preparation procedure is illustrated in Scheme 1.

Preparation of the PMA-APM-r-PS Copolymer Films

Microporous films were prepared by casting the 30 wt % PMA-APM-r-PS copolymer solution in tetrahydrofuran (THF) at room temperature in a glove box under a nitrogen atmosphere onto a variety of substrates, such as glass slides, aluminum plates, metal wafers, and mica.

Characterization

The molecular weight of the raw sample and its distribution were determined by gel permeation chromatography (GPC), using a Postnova 1021 solvent delivery pump, Viscotek 270 dual detector, Viscotek VE 3580 RI detector, and American Polymer Standards Corporation 10 μm AM Gel GPC columns (AM Gel 10^3Å, 10^4Å, and 10^5Å) with linear polystyrene (PS) standards. THF (HPLC grade) was used for elution at a flow rate of 1 mL/min. The GPC results were calibrated according to conventional calibration methods (CC). ^{1}H NMR and ^{13}C NMR spectra were recorded using a Bruker 400-MHz FT-NMR instrument, and the chemical shifts were recorded in parts per million with tetramethylsilane as an internal standard. Fourier transfer infrared (FTIR) spectra were recorded using a Varian 2000 FTIR analyzer, which was operated from 700 to 4000 cm^{-1} at room temperature. FTIR spectra were obtained using a resolution of 4 cm^{-1} and were averaged over 32 scans. The samples were thoroughly mixed with potassium bromide (KBr) at approximately 3 wt %, and the resulting powders were pressed into a transparent pellet. Elemental analysis (EA) was performed using an Elementar Vario EL III elemental analyzer and X-ray photoemission spectrometry (XPS) was performed using a Kratos Axis Ultra DLD ESCA machine. The thermal properties of the polymers were measured by thermogravimetric analysis (TGA) performed using a TA TGA-Q50 thermogravimetric analyzer. Samples were heated from room temperature to 800 °C at a heating rate of 20 °C/min in a nitrogen purge system. T_g was determined by DSC from the midpoint of the inflection tangent with a second heating at 10 °C/min. TGA and DSC data were analyzed using TA Instruments Universal Analysis software. A Hitachi S4200 field emission scanning electron microscope (FE-SEM) was used to observe the morphology of the dendritic-linear PMA-APM-r-PS copolymer.

RESULTS AND DISCUSSION

Synthesis and Characterization

Synthesis of the MA-APM Dendritic Macromonomer

Preparation of the dendritic-linear copolymers can be carried out in a number of ways, including: (a) polymerization of the dendron-functionalized macromonomers, (b) grafting of dendrons to a linear polymer backbone, or (c) divergent dendronization of appropriately functionalized linear polymers. In this research, we used a combination of methods (a) and (b) to obtain our dendritic-linear copolymers. The MA-APM dendritic macromonomer was directly synthesized by subjecting it to a ring-opening reaction and repeated alkylation and amidation using a divergent growth approach. It was then ultimately polymerized with a styrene monomer.

Synthesis of the MA-APM Macromonomer

Dendritic MA-APM macromonomers were synthesized according to Scheme 1, and characterized by ^{1}H NMR, ^{13}C NMR, and FTIR, respectively. Figure 1 presents the FTIR spectra of the MA monomer, MA-APM-G0.5 and MA-APM-G1 macromonomer signals. The MA-APM-G0.5 spectrum depicted in Figure 1(b) indicates that signals at 1853 cm^{-1} and 1782 cm^{-1}, corresponding to the symmetric and asymmetric stretching vibrations of C=O, cannot be observed; however, three significant peaks at 1696, 1658, and 1546 cm^{-1}, corresponding to the stretching vibrations of C=O in the carboxylic acid group, amide I band, and amide II band, can be observed. These peaks demonstrate that the ring of the MA monomer is opened and that the dendritic MA-APM-G0.5 was successfully synthesized. Furthermore, as the generation of the dendritic MA-APM macromonomer increases from [G = 0.5] to [G = 1], we can see in Figure 1(b) the

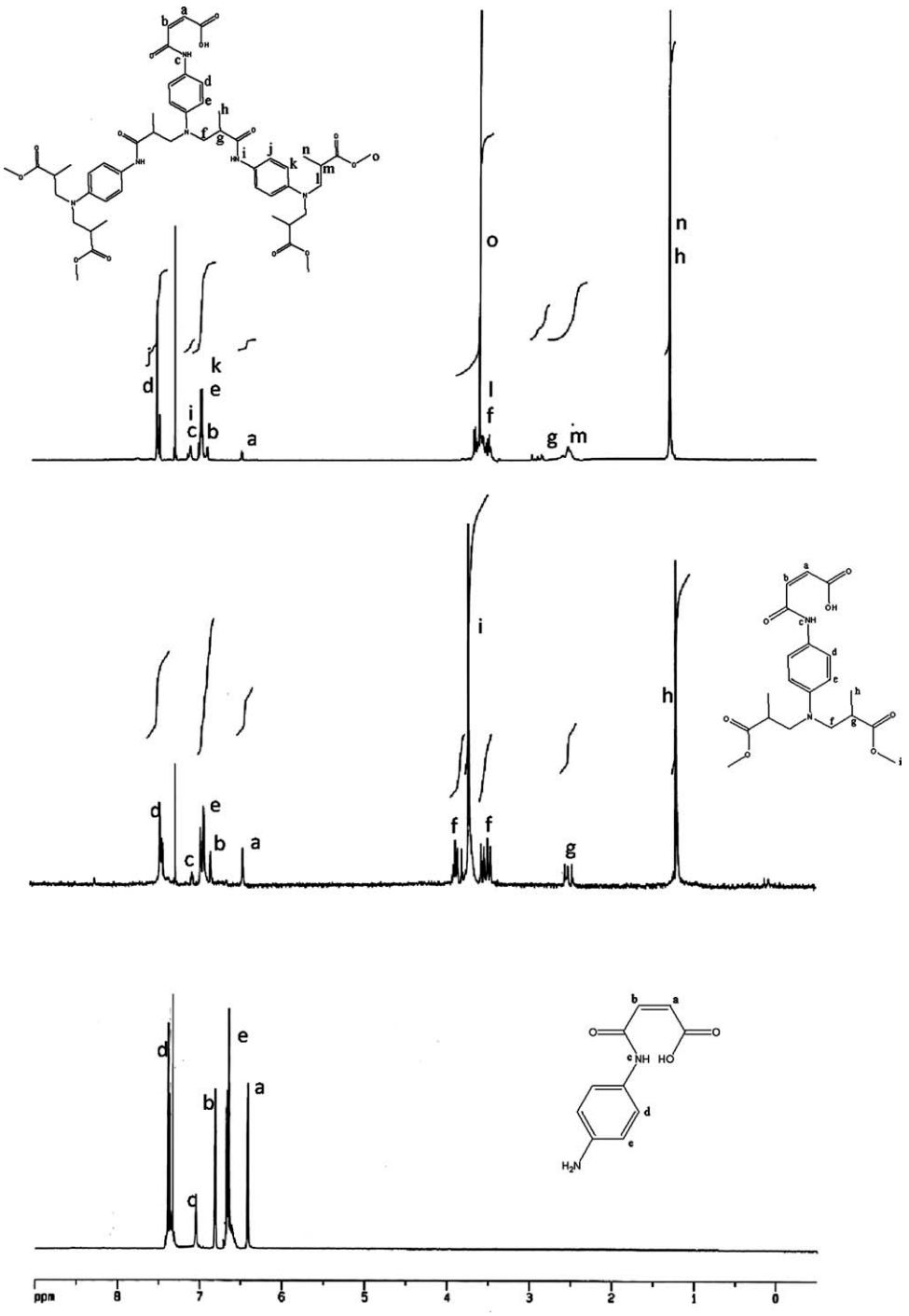

FIGURE 2 ^{1}H NMR spectra of (a) MA-APM-G0.5, (b) MA-APM-G1.0, and (c) MA-APM-G2.0 in $CDCl_3$.

clear characteristic peak at 1740 cm^{-1} that corresponds to the stretching vibrations of C=O in the ester. Moreover, the C=C stretching vibration signal of the macromonomer at 1640 cm^{-1} still exists in each generation of the dendritic MA-APM macromonomer.

Figure 2 depicts 1H NMR spectra of the dendritic MA-APM-G0.5, MA-APM-G1.0, and MA-APM-G2.0 macromonomers. The formation of the amine-terminated MA-APM-G0.5 macromonomer proceeded as expected with the addition of *p*-phenylenediamine to the Maleic anhydride. The ester-terminated MA-APM-G1.0 macromonomer was synthesized by reacting the amine-terminated MA-APM-G0.5 macromonomer with methyl methacrylate, and the higher generation dendritic macromonomers were obtained by repeating the procedure. The ^{1}H NMR spectra of the dendritic MA-APM-G0.5 and MA-APM-G1.0 macromonomers [Fig. 2(a,b)], as well as a significant appearance of methyl ester protons (—OCH_3—) at 3.69 ppm during the formation of the ester-terminated MA-APM-G1 dendritic macromonomer, indicate that close to a 100% substitution occurred for each generation. The chemical shift

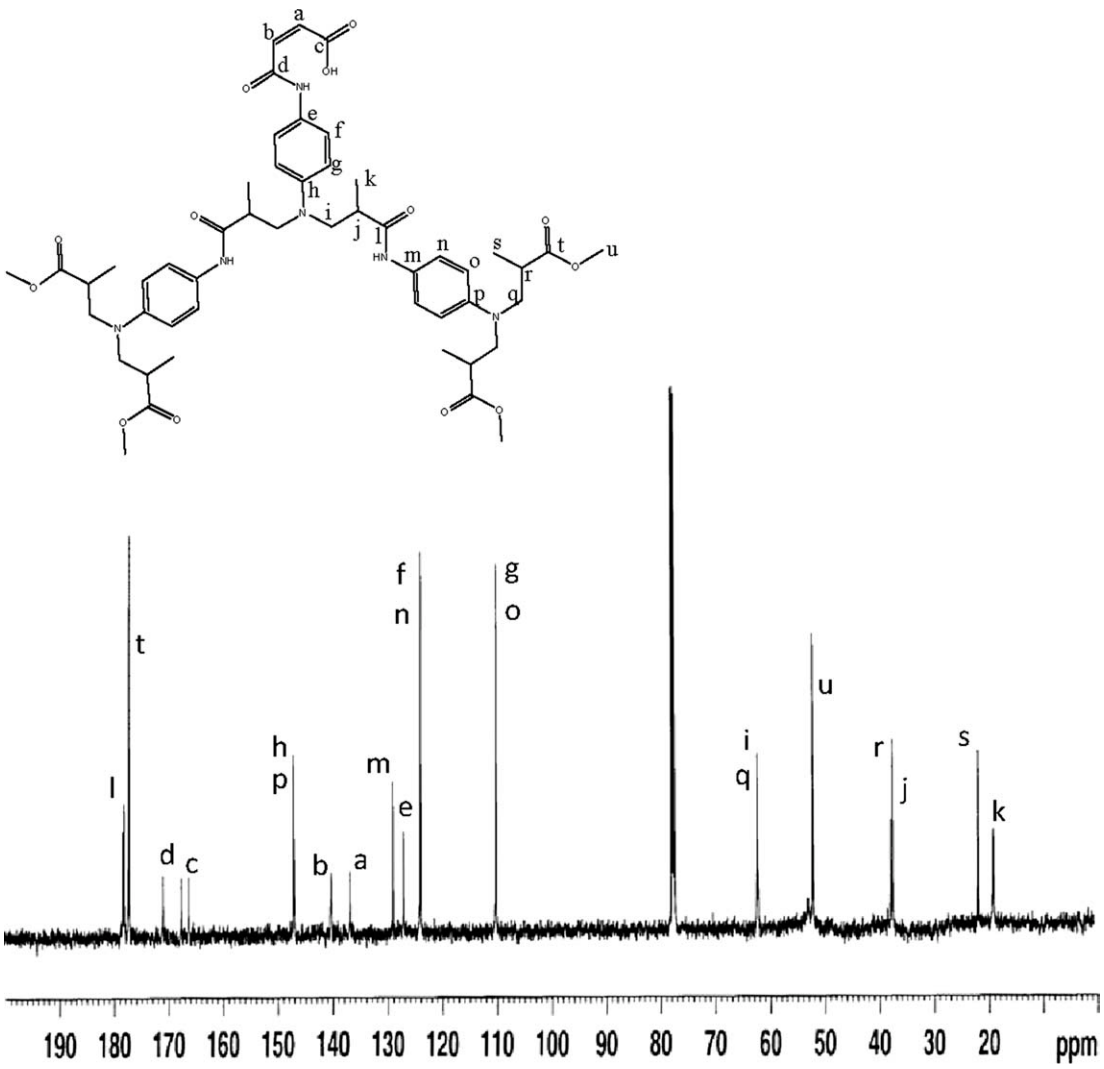

FIGURE 3 ^{13}C NMR spectrum of the G2 MA-APM in $CDCl_3$.

of the proton in the amide group (—CO—N*H*—) is apparent at 7.08 ppm, and the chemical shifts of the proton in the phenyl group (N-Ar*H*-N) are apparent at 6.90 ppm and 7.39 ppm, respectively. In addition, the chemical shifts of the protons from the double bond (CH_2=C—) are significantly apparent across the different generations at 6.42 and 6.85 ppm, respectively. The integration values of these signals can be used to determine the arm number of the dendritic macromonomer. On the basis of the calculated results, the MA-APM dendritic macromonomers were defined as MA-GX, where *X* indicates the number of generations associated with the MA-APM dendritic macromonomer. Therefore, G2 represents the second generation and has four arms of the methyl ester group in the dendritic macromonomer. Furthermore, the ^{13}C NMR spectrum of the MA-APM macromonomer (Fig. 3) features double bond (C=C) signals at 136.3 and 138.8 ppm, respectively. Signals related to the carboxylic acid structures appear at 166.2 ppm. This result is consistent with the notion that the ring of the MA monomer is opened. Therefore, the MA-APM macromonomer was successfully synthesized as identified via 1H NMR, ^{13}C NMR, and FTIR.

Synthesis of the Dendritic-Linear PMA-APM-r-PS Copolymer

The dendritic-linear PMA-APM-r-PS copolymers were synthesized via free radical polymerization involving the styrene monomer and the dendritic MA-APM macromonomer. The products were characterized by ^{1}H NMR, ^{13}C NMR, and EA.

Figure 4 depicts the ^{1}H NMR and ^{13}C NMR spectra for the dendritic-linear PMA-APM-r-PS copolymer. ^{1}H NMR was used to determine the content of the dendritic MA-APM segment for the dendritic-linear PGMA-HPAM-r-PS copolymer by comparing the peak integration values. Specifically, the integration value from the dendritic MA-APM segment ester group (—CO—OCH_3), which was apparent at around 3.69 ppm, was compared to the integration values from the proton of the amide group (—CO—NH—), consistent with chemical shifts in the dendritic MA-APM segment at 7.08 ppm. We also took

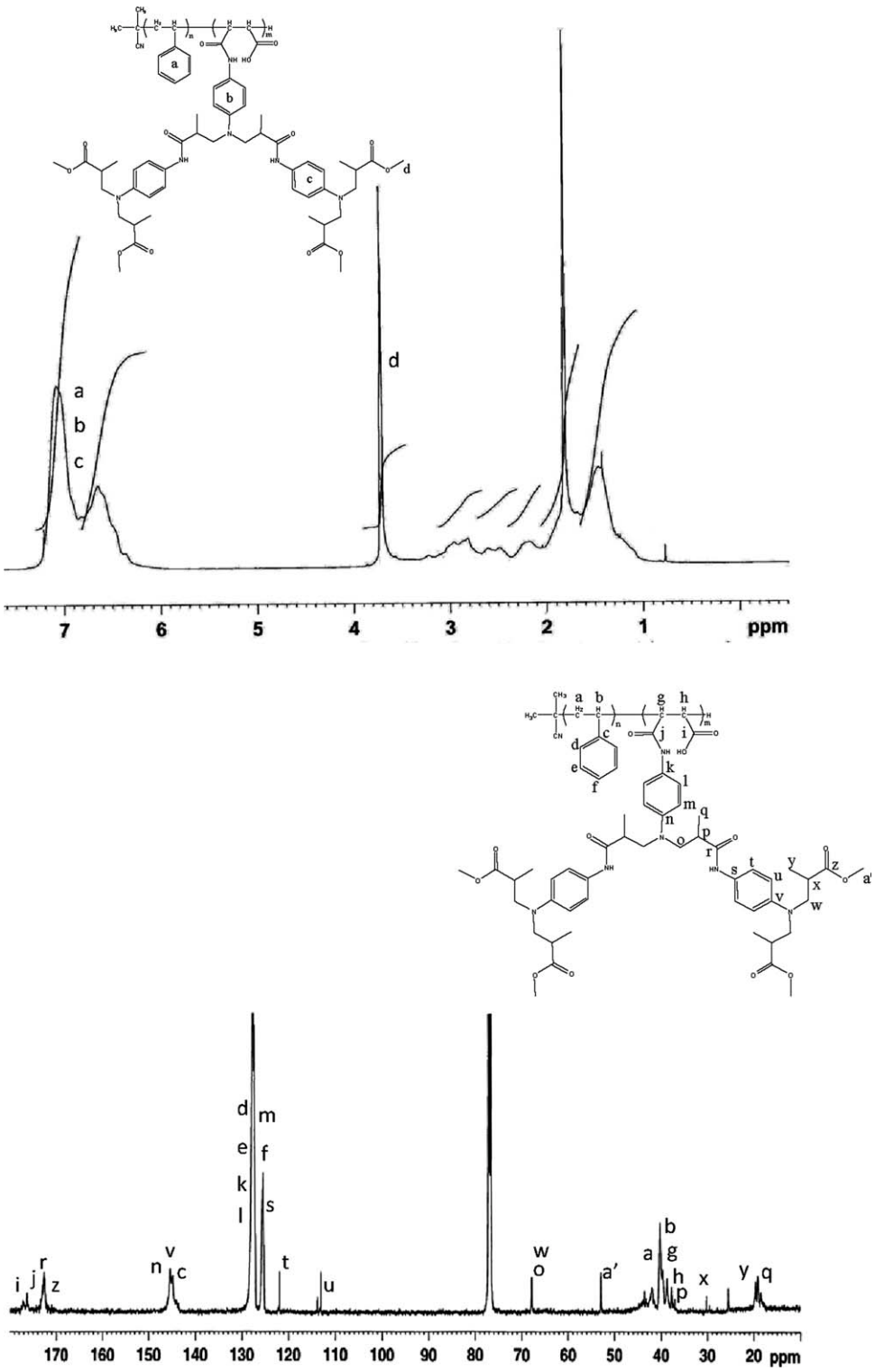

FIGURE 4 (a) ^{1}H NMR and (b) ^{13}C NMR spectra of the dendritic-linear PMA-APM-r-PS copolymer in $CDCl_3$.

into account the phenyl group's chemical shift in the context of the styrene segment and the dendritic MA-APM segment at 6.6–7.4 ppm. On the basis of the calculated results, the dendritic-linear PMA-APM-r-PS copolymers were defined as MG2-Y, where *Y* represents the weight percentage of the dendritic MA-APM segment in PMA-APM-r-PS copolymers. Therefore, MG2–15 represents the second generation dendritic macromonomer in each dendritic segment, and accounts for 15 wt % of the entire dendritic-linear PMA-APM-r-PS copolymer. The series of percentages in this research includes MG2–15, MG2–23, MG2–34, MG2–43, MG2–49, and MG2–54. Moreover, the results of the elemental analysis, as listed in Table 1, do seem to confirm the weight percentage of the dendritic segments for each PMA-APM-r-PS copolymer. From

TABLE 1 PMA-APM-r-PS Molecular Characteristics and Morphology

Designation (Generation no. – MA-APM Segment wt %)	MA-APM-Segment wt %[a]	M_w[b] (10^3 g/mol)	PDI	Morphology (SEM)	Elemental Analysis		
					C%	N%	H%
MG2-macromonomer	–	0.958[a]	–	–	62.58	8.87	6.91
MG2–15	14.6	45.4	1.957	Phase separation/disordered	87.88	1.32	7.54
MG2–23	23.2	36.6	1.864	Phase separation/disordered	85.96	1.89	7.48
MG2–34	34.1	28.1	1.794	Phase separation/pseudo-disordered	83.72	2.56	7.40
MG2–43	42.9	31.8	1.813	Phase separation/honeycomb-ordered	82.14	3.02	7.35
MG2–49	49.4	35.3	1.878	Phase separation/disordered	81.19	3.30	7.31
MG2–54	53.8	41.6	2.103	Phase separation/disordered	80.47	3.52	7.29

[a] Calculated by ^{1}H NMR

[b] Determined by GPC

the ^{13}C NMR analysis depicted in Figure 4(b), we note the chemical shift at 38 ppm, which is linked with the main chain —C—C— bonds of the styrene segment. These data may indicate the formation of the PMA-APM-r-PS copolymer.

Table 1 summarizes GPC results for the PMA-APM-r-PS copolymers, with the data calibrated according to conventional calibration methods (CC) and using linear polystyrene standards. The polydispersity indexes (PDI) of the PMA-APM-r-PS copolymers seem slightly broadened, around 1.82.2. This phenomenon can be ascribed to the structure of the dendritic-linear copolymers, because of their different hydrodynamic volumes[28,29] and side chain effects,[30–33] in comparsion to a linear polymer of the same molecular weight.

XPS was utilized to analyze the compositions of the PMA-APM-r-PS copolymer samples. In each case, a broad initial scan was performed (1100–0 eV) to establish the gross elemental composition on the surface of the samples. The PMA-APM-r-PS membranes exhibited distinct carbon (C 1s, C KLL), oxygen (O 1s, O KLL) and nitrogen (N 1s) peaks, representing the major constituents of the sample surface; however the N 1s peak at a binding energy of around 400 eV, which reflects the presence of the amine structure,[34] confirms the structure of the PMA-APM-r-PS membranes. The results of the XPS experimental data are consistent with the FTIR analysis and ^{1}H NMR spectra. Furthermore, detailed analysis of the XPS spectra offers clear evidence that the dendritic PMA-APM-r-PS copolymers were successfully synthesized. Before discussing the C 1s spectra, it is important to note that the short-range nature of substituent effects can lead to additive rules for the C 1s shift.[35] Thus, the degree of shifting of the characteristic peak for the C 1s of carbon, which is single bonded to oxygen (alcohols, ethers, and esters), is about 1.6 eV.[35] For carbon that is single bonded to two oxygen atoms, the degree of shifting of the characteristic peak for C 1s is about 2.8 eV, approximately twice the effect of a single substituent. For carbon double bonded to oxygen in simple carbonyl compounds, the characteristic shift is about 2.6 eV.[36] For a carbonyl to carbonyl group, there is a 1.4 eV change in binding energy associated with the additional oxygen that is single bonded to carbon. This yields a total shift of about 4 eV.[36] Moreover, the shift arising from replacing a carbon or hydrogen with a nitrogen that is directly attached to the carbon atom under consideration is about 1 eV.[35] As can be seen in Figure 5(a), the C 1s signal of the PMA-APM-r-PS copolymer can be decomposed into four peaks. The peaks located at 283.7–285.4 eV, according to the internal energy standard, can be interpreted as the combination of the sp^2 C=C and sp^3 C—C structures of the bulk and surface carbons of the PMA-APM-r-PS copolymers. The peak at 286.4–286.6 eV originates from the —C—N— and —C—O—, and the peak at 288.8–289.4 eV is associated with —C(=O)—N— and —C(=O)—O— structures. The last peak located at 292.3 eV represents the shake-up structure associated with π to π^* transitions of the phenyl rings.

Figure 5(b) shows that the N 1s peak is composed of two peaks, located at 399.7, and 399.9 eV, which originate from the —C(=O)—NH—, and Ar-N structures, respectively. Furthermore, the O 1s peak at 532.1 eV in Figure 5(c) is attributed to C=O in the —C(=O)—N and —C(=O)—O structures, and the peak at 533.7 is associated with C—O, including C(=O)—OH and C(=O)—O—C structures. These graphs provide evidence that the dendritic PMA-APM-r-PS copolymers were successfully synthesized, and these data are consistent with the above NMR and FTIR results.

A review of the experimental FTIR, ^{1}H NMR, ^{13}C NMR, and GPC results reveals that the dendritic macromonomer and the dendritic-linear PMA-APM-r-PS copolymers were successfully synthesized in this study. For each MG2-X copolymer, Table 1 lists the generation number, molecular weight, weight percentage of the dendritic MA-APM segment, PDI, and elemental analysis results.

Thermal Behavior

TGA and DSC analyses were used to determine the thermal properties of the dendritic-linear PMA-APM-r-PS copolymer. TGA is a technique used to accurately track the *in situ* weight changes of the sample during heating. Figure 6 shows the TGA thermograms of the various PMA-APM-r-PS

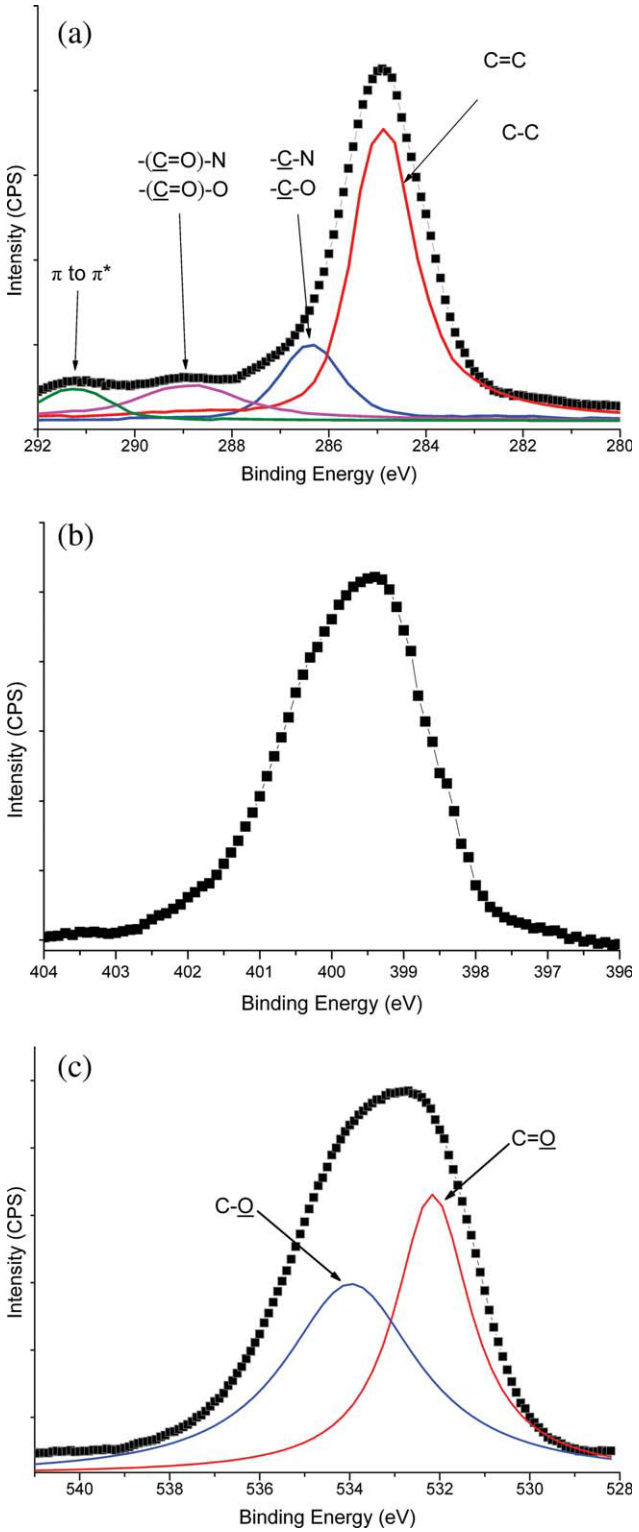

FIGURE 5 XPS core level spectra of (a) C 1s, (b) N 1s, and (c) O 1s of the PMA-APM-r-PS copolymer.

copolymers, notated as PS, MG2–15, MG2–23, MG2–34, MG2–43, MG2–49, and MG2–54. The dendritic segments (MA-APM) have a significant effect on the resulting dendritic-linear PMA-APM-r-PS copolymers in comparsion to the PS homopolymer in the thermal decomposition.[36–38] When polymerized with the dendritic segment (MA-APM) at 15 wt %, the thermal degradation temperature of the dendritic-linear copolymer is 39 °C higher at 360 °C than would be the case for the PS homopolymer at 321 °C (curves a and b in Fig. 6). As a function of increasing dendritic segment (MA-APM) wt %, the thermal degradation temperature of the dendritic-linear PMA-APM-r-PS copolymer was elevated by 38 °C from 360 °C for MG2–15 to 398 °C for MG2–54. In addition, we note that the dendritic-linear MG2–54 copolymer (PMA-APM-r-PS) is thermally stable up to 398 °C.

On the other hand, the thermal behaviors of the PMA-APM-r-PS copolymers were monitored using differential scanning calorimetry (DSC), as shown in Figure 7. Theoretically, the glass transition temperature (T_g) of the copolymers should decrease with increased branching. We considered the fact that the presence of a side group is known to influence the T_g of a particular copolymer by an amount that depends on the flexibility and bulk of the side group. Usually, flexible side chains and/or pendent groups increase the flexibility of the backbone chain and lead to a decrease in the glass transition temperature. In principle, the glass transition of carbon-backbone copolymers reflects the rotational energy barriers about σ bonds of the main chain and lower glass transition temperatures resulting from lower energy barriers. While the dominating effect of flexible side chains is to increase free volume, thus lowering T_g, the rigid side chains may restrict torsion about σ bonds in the main chain, increasing T_g. In our system, the dendritic MA-APM segment, which has a high degree of extension and three-dimension structure, can be undoubtedly considered a flexible group. Therefore, the T_g value also depends on the free volume of the dendritic segment of the PMA-APM-r-PS copolymers. In the MG2-X system, for polymerization with the dendritic segment (MA-APM) at a 15 wt % content, the glass transition temperature of the dendritic-linear copolymer is significantly lower than would be the case for the PS homopolymer: we note a 7 °C decrease, from 94 to 87 °C [curves a and b in Fig. 8(a)]. By increasing the

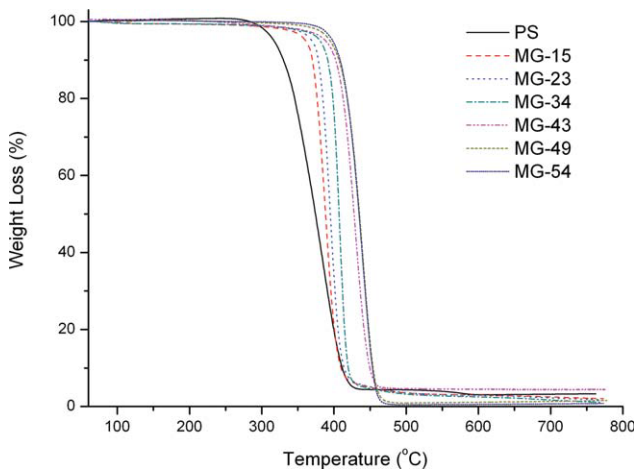

FIGURE 6 TGA curves of the (a) MG2-X PMA-APM-r-PS series copolymers.

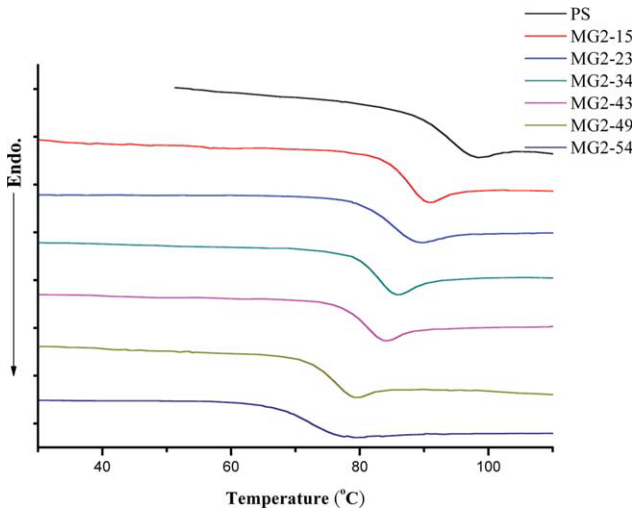

FIGURE 7 DSC curves of the (a) MG2-X PMA-APM-r-PS series copolymers. [Color figure can be viewed in the online issue, which is available at www.interscience.wiley.com.]

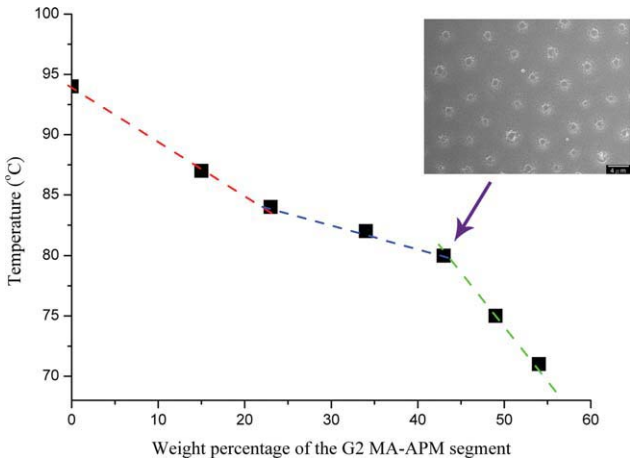

FIGURE 8 Variation of glass transition temperature (T_g) for the G2 dendritic-linear PMA-APM-r-PS copolymers as a function of the G2 dendritic MA-APM segment content. [Color figure can be viewed in the online issue, which is available at www.interscience.wiley.com.]

dendritic segment (MA-APM) contents, the T_g value of the dendritic-linear PMA-APM-r-PS copolymers decreased by 16 °C, from 87 °C for MG2–15 to 71 °C for MG2–54. The reduced degree of the T_g value in the PMA-APM-r-PS system is more less than that of the PGMA-HPAM-r-PS system reported in our previous report, which is due an increase in the number of phenyl groups in the MA-APM structure that make the flexibility and mobility lower than that of the GMA-HPAM structure. For each dendritic-linear PMA-APM-r-PS copolymer, the decomposition temperature (T_d) and the glass transition temperature (T_g) are listed in Table 2.

Furthermore, we were able to use the variation of the glass transition temperature to quickly find the critical equilibrium, which resulted in the hexagonally-ordered microporous structure in our previously reported PGMA-HPAM-r-PS system. In the MG-X system, we still found three trends in the wt % plot of the dendritic MA-APM vs. glass transition temperature (T_g) depicted in Figure 8. The first trend occurred at 0–23 wt %, and second at 23–43 wt % and third at 43–54 wt %. The variation of T_g in the dendritic-linear PMA-APM-r-PS copolymers results from two effects: the free volume of the dendritic segment and the interaction of the dendritic and styrene segments. Because the dendritic MA-APM segments are flexible structures, they are expected to increase the free volume, lowering T_g. A manifested decrease in T_g at the lower content of the dendritic MA-APM segment (the first trend) was observed. When the weight percentage of the dendritic MA-APM segment was set to a specific value, the intermolecular interactions between each segment were significant enough to affect copolymer chain motion and result in an enhancement in T_g. Therefore, the change in T_g, influenced by the free volume and intermolecular interactions, begin to flatten out (the second trend). Moreover, we can observe an ordered structure on the copolymer film surface when the interaction between the dendritic segment and the styrene segment approximately reach a critical equilibrium (the intersection). Afterward, the balance between each segment is slightly disrupted, leading the variation of the T_g to a different condition (the third trend). This phenomenon coincides with the copolymer morphology observed via SEM, which is discussed later.

Polymer Morphology

Our dendritic-linear PMA-APM-r-PS microporous copolymer films were prepared at room temperature by casting the THF solution onto the substrate. Figure 9 depicts SEM images of the microporous PMA-APM-r-PS copolymer films with different dendritic MA-APM segment contents. In particular, the formation of ordered packed micropores with a uniform size distribution can be observed for MG2–43 in the SEM images depicted in Figure 9. The formation mechanism of the ordered/disordered microporous surface structures has been described in our previous report. The resulting micropores in the self-assembled film matrix can be ascribed to the aggregation of the dendritic MA-APM segment of the dendritic-linear PMA-APM-r-PS copolymer. The continuous or dispersed condition of each styrene and dendritic segment micelle control the surface morphologies of the PMA-APM-r-PS copolymer films. In this case, because the entanglement and mobility of the dendritic MA-APM segment are constrained by the main chain in the

TABLE 2 The Thermal Stability of PMA-APM-r-PS

Sample	Dendron	T_d[a] (°C)	T_g[b] (°C)
PS	–	321	94
MG2–15	G2	360	87
MG2–23	G2	369	84
MG2–34	G2	380	82
MG2–43	G2	388	80
MG2–49	G2	394	75
MG2–54	G2	398	71

[a] Condition: Heating rate 20 °C/min under N_2 purge.
[b] Condition: Heating rate 10 °C/min, under N_2 purge.

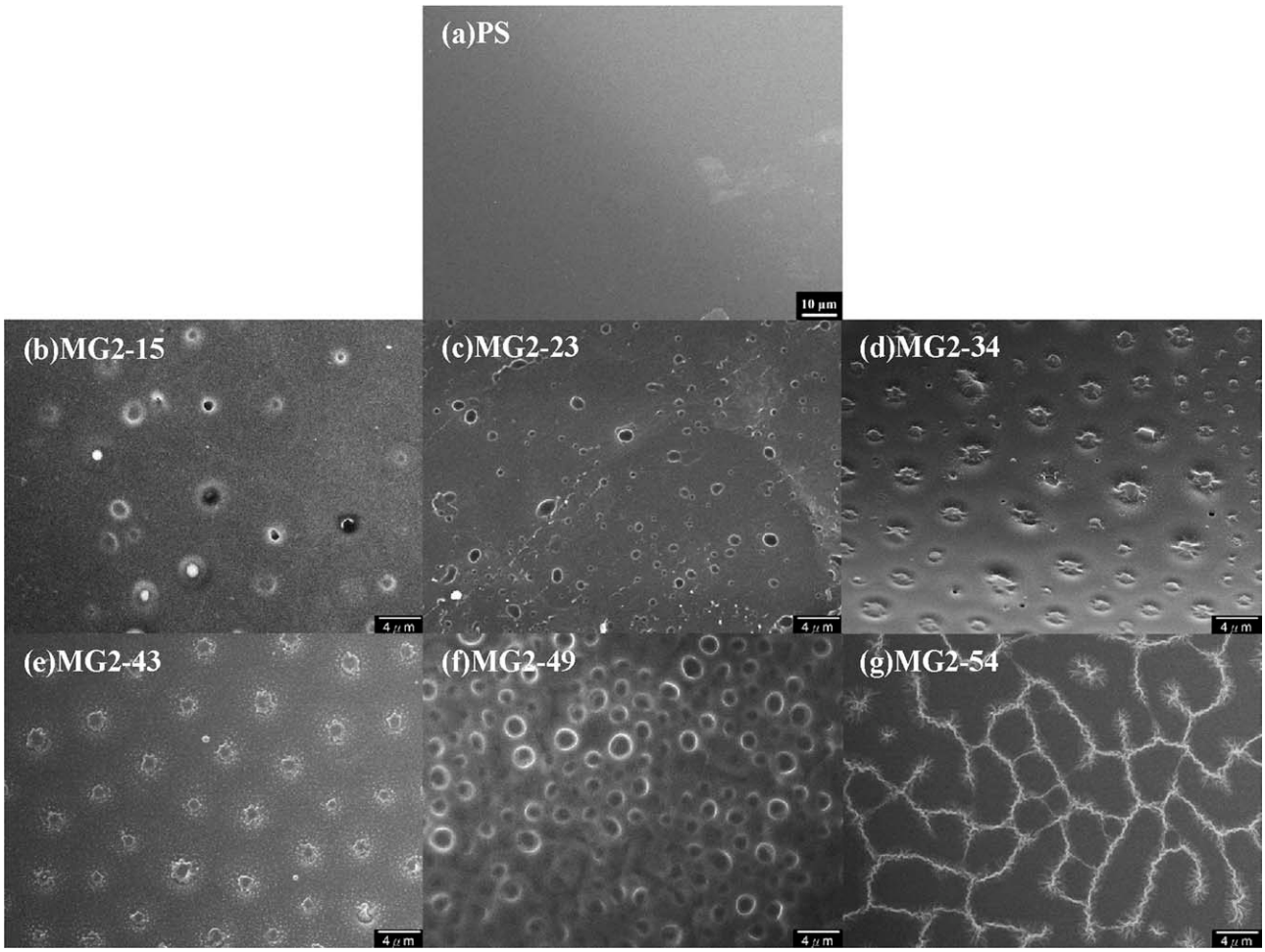

FIGURE 9 SEM photographs of the microporous PMA-APM-r-PS copolymer film given different dendritic MA-APM segment contents. (a) PS, (b) MG2–15, (c) MG2–23, (d) MG2–34, (e) MG2–43, (f) MG2–49, and (g) MG2–54.

PMA-APM-r-PS copolymer, the shapes and the volumes of the dendritic MA-APM segment micelle domains are related to the number of styrene segments in solution. The dendritic MA-APM segment domains should prefer to form spherical shapes, consistent with thermodynamics, because the styrene segment content is much greater than the dendritic segment content. It follows that the PMA-APM-r-PS copolymer films, which exhibit a spherical microporous matrix, are formed after solvent evaporation, as shown in the SEM images. With several different dendritic segment contents, this formation mechanism can be categorized into three routes: (i) the morphologies of the PMA-APM-r-PS copolymer films are controlled by the continuous phase of the styrene segment in the copolymers; (ii) the surface morphologies of the PMA-APM-r-PS copolymer films are gradually affected by the dendritic segment micelles; and (iii) surface data regarding the PMA-APM-r-PS copolymer films are jointly controlled by the styrene and the dendritic segments. As shown in the SEM photographs, the average diameters of the self-assembled micropores were estimated to range from 1.9 μm to 2.5 μm for the MG2–43 system. Moreover, the average interval distance of the ordered-array structures in the MG2–43 system was found to range from 5.1 to 5.4 μm, respectively. From these results, we can calculate the volumetric fraction of the hexagonally-ordered structures in the dendritic-linear PMA-APM-r-PS film. According to the literature,[39,40] the relationship between volumetric fraction (φ), radius (R) and repeating distance (L) of ordered arrays is given by:

$$\varphi = \pi\left(\frac{R}{L}\right)^2$$

Given that L = 5–5.4 μm and R = 0.95–1.25 μm, the volumetric fraction of the micropores φ is 0.11 to 0.17 for the MG2–43 system. The dendron is a dimensional architecture, and its configuration can be broadly reworked and reinterpreted. This may explain the values of the volumetric fractions for MG2–43. Additionally, the morphologies of the various dendritic proportions of the PMA-APM-r-PS MG2-X copolymers are listed in Table 1.

CONCLUSION

New kinds of dendritic MA-APM macromonomer and dendritic-linear PMA-APM-r-PS copolymers were successfully synthesized by a coupling reaction using the divergent method. ^{1}H NMR, ^{13}C NMR, FTIR, EA, and XPS analyses confirmed the

structure and characteristics of the MA-APM macromonomers and the PMA-APM-r-PS copolymers. In addition, microporous structure films were successfully manufactured by casting a series of the PMA-APM-r-PS copolymers and using a THF solution at room temperature via the solution induced phase separation method. Of note, at 43 wt % of the dendritic MA-APM segments in the MG2–43 copolymer, the dendritic segment micelle displayed self-assembling behavior that resulted in a ordered-array microporous copolymer matrix. Our research confirms that controlling the appropriate macromonomer content via the grafting of a three-dimensional structure, like MA-APM, can promote self-assembly and produces a ordered-array microporous copolymer matrix.

We gratefully acknowledge the financial support of the Ministry of Economic Affairs of the Republic of China (TDPA: 97-EC-17-A-05-S1-0014) and the National Science Council (NSC: 97-2221-E-006-100-MY3).

REFERENCES AND NOTES

1 Tabu, H.; Shimomura, M. Langmuir 2005, 21, 1709–1711.

2 Ballew, H. W. Am Biotechnol Lab 1997, May, 8.

3 Gupta, S.; Tuttle, G.; Sigalas, M.; Ho, K. M. Appl Phys Lett 1997, 71, 2412–2414.

4 Judith, E. G.; Wijnhoven, J.; Willem, L. V. Science 1998, 281, 802–804.

5 Müller, M.; Zentel, R.; Maka, T.; Romanov, S. G.; Torres, C. M. S. Adv Mater 2000, 12, 1499–1503.

6 Fichet, G.; Cororan, N.; Ho, P. K. H.; Arias, A. C.; MacKenzie, J. D.; Huck, W. T. S.; Friend, R. H. Adv Mater 2004, 16, 1908–1912.

7 Deleuze, H.; Schultze, X.; Sherrington, D. C. Polymer 1998, 39, 6109–6114.

8 Kasemo, B. Surf Sci 2002, 500, 656–677.

9 Moreau, W. M. Semiconductor Lithography: Principles and Materials; Plenum: New York, 1998.

10 Oberdisse, J.; Deme, B. Macromolecules 2002, 35, 4397–4405.

11 Mayer, A. B. R.; Grebner, W.; Wannemacher, R. J Phys Chem B 2000, 104, 7278–7285.

12 Galloro, J.; Ginzbug, M.; Míguez, H.; Yang, S. M.; Coombs, N.; Safa-Sefat, A.; Greedan, J. E.; Manners, I.; Ozin, G. A. Adv Funct Mater 2002, 12, 382–388.

13 Hong, J. C.; Park, J. H.; Chun, C.; Kim, D. Y. Adv Funct Mater 2007, 17, 2462–2469.

14 Widawski, G.; Rawiso, M.; Francois, B. Nature 1994, 369, 387–389.

15 Jenekhe, S. A.; Chen, X. L. Science 1999, 283, 372–375.

16 Srinivasarao, M.; Collings, D.; Philips, A.; Patel, S. Science 2001, 292, 79–83.

17 Song, L.; Bly, R. K.; Wilson, J. N.; Bakbak, S.; Park, J. O.; Srinivasarao, M.; Bunz, U. H. F. Adv Mater 2004, 16, 115–118.

18 Zhang, Y.; Wang, C. Adv Mater 2007, 19, 913–916.

19 Stenzel, M. H.; Kowollik, C. B.; Davis, T. P. J Polym Sci Part A: Polym Chem 2006, 44, 2363–2375.

20 Schlüter, A. D.; Rabe, J. P. Angew Chem Int Ed Engl 2000, 39, 864–883.

21 Grayson, S. M.; Fréchet, J. M. J Chem Rev 2001, 101, 3819–3867.

22 Percec, V.; Heck, J.; Tomazos, D.; Falkenberg, F.; Blackwell, H.; Ungar, G. J Chem Soc Perkin Trans 1 1993, 1, 2799–2811.

23 Cheng, C.; Tian, Y.; Shi, Y.; Tang, R.; Xi, F. Macromol Rapid Commum 2005, 26, 1266–1272.

24 Ishizu, K.; Makino, M.; Uchida, S. Macromol Ropid Commum 2007, 28, 882–887.

25 Hsieh, S. J.; Wang, C. C.; Chen, C. Y. Macromolecules 2009, 42, 4787–4794.

26 Tercjak, A.; Serrano, E.; Garcia, I.; Ocando, C.; Mondragon, I. Acta Mater 2007, 55, 6436–6443.

27 Ishizu, K.; Tokuno, Y.; Makino, M. Macromolecules 2007, 40, 763–765.

28 Hawker, C. J.; Malmström, E. E.; Frank, C. W.; Kampf, J. P. J Am Chem Soc 1997, 119, 9903–9904.

29 Jahromi, S.; Palmen, J. H. M.; Steeman, P. A. M. Macromolecules 2000, 33, 577–581.

30 Kasko, A. M.; Heintz, A. M.; Pugh, C. Macromolecules 1998, 31, 256–271.

31 Levine, A. J.; Milner, S. T. Macromolecules 1998, 31, 8623–8637.

32 Förster, S. Macromolecules 1999, 32, 4043–4049.

33 Chou, C.-H.; Shu, C.-F. Macromolecules 2002, 35, 9673–9677.

34 Solomum, T.; Schimanski, A.; Sturm, H.; Illenberger, E. Macromolecules 2005, 38, 4231–4236.

35 Clark, D. T.; Thomas, H. R. J Polym Sci 1978, 16, 791–820.

36 Clark, D. T.; Thomas, H. R. J Polym Sci Polym Chem Ed 1976, 14, 1671–1700.

37 Jiang, G.; Wang, L.; Chen, T.; Yu, H. Polymer 2005, 46, 81–87.

38 Jiang, G.; Wang, L.; Chen, T.; Wang, J.; Chen, C.; Yu, H. J Appl Polym Sci 2005, 98, 1106–1112.

39 Matsen, M. W.; Bates, F. S. Macromolecules 1996, 29, 1091–1098.

40 Rider, D. A.; Cavicchi, K. A.; Power-Billard, K. N.; Russell, T. P.; Manners, I. Macromolecules 2005, 38, 6931–6938.